The search for P-waves at Forties

Jason P. Chang

ABSTRACT

Results from seismic interferometry at Apache Forties indicates the presence of P-wave events hidden in the ambient seismic noise field. I use phase-weighted stacking rather than linear stacking of correlations from quiet time periods to enhance this apparent P-wave energy. From source gathers with a virtual source located near the platform, there are three apparent events in the hydrophone-hydrophone and vertical-vertical geophone correlations between 40 and 80 Hz. From a tau-p transform of these gathers, there are events in the hydrophone component propagating at 1500 m/s and 3000 m/s with 0 s intercept time, while in the vertical-geophone component there are two events propagating at 3000 m/s with different intercept times. To determine the direction in which these events are traveling through the array, I look at source gathers along approximate lines of receivers in the north-south, east-west, and northeast-southwest directions. Using linear moveout with velocity estimated from the tau-p transform, I find that the slower event in the hydrophone correlations appears to be moving across the array from generally northeast to southwest, while the faster events in both component correlations appear to propagate from the platform. Based on the unlikelihood of interface waves traveling at such high velocities, I perform passive fathometry processing on ambient noise records in an attempt to recover body-wave energy. Preliminary results of passive fathometry appear to retrieve the water-column multiple along with some possible reflection events.

INTRODUCTION

Utilization of the interface-wave portion of Earth's ambient noise field to image the subsurface has been successful at the continental, regional, and local scales (e.g., Shapiro et al., 2005; Bensen et al., 2008; de Ridder and Dellinger, 2011). As a result, focus has shifted to extracting the body-wave portion of the Earth's ambient noise field for imaging. At the local scale and on land, Nakata et al. (2011) and Draganov et al. (2013) were able to recover reflection events from passive seismic data. Additionally, Nakata et al. (2015) was able to recover diving P-waves using a dense array at Long Beach, California, which were subsequently used to produce a 3-dimensional tomographic image of the subsurface. There has been similar success in finding non-interface waves in shallow marine ambient noise fields. Using continuous recordings from an ocean-bottom cable network in the Valhall oil field, Mordret et al. (2013) extracted an apparent acoustic wave generated by an operating platform. Brooks

and Gerstoft (2009) extracted direct, sea-surface reflected, and sea-bottom reflected events in the water column from shipping and wave noise recorded by a small L-shaped (vertical and horizontal) hydrophone array in offshore New Jersey. Using a technique called passive fathometry, numerous studies (e.g., Gerstoft et al., 2008; Siderius et al., 2010) obtained shallow subsurface reflection images using energy generated by breaking waves at the sea surface recorded by a vertical array in the water column.

Here, I build off results from Chang (2016), who used seismic interferometry processing to extract P-waves that appeared to be propagating from the platform at Apache Forties. The goal of this report is to better classify the apparent P-waves in the hydrophone-hydrophone and vertical-vertical geophone correlations, and to determine whether these events can be used to image the subsurface. First, I introduce the continuous recordings from the Apache Forties dataset. Second, I apply seismic interferometry processing with phase-weighted stacking to generate high-frequency virtual source gathers throughout the array. To get a sense of velocities of the events, I perform a tau-p transform. To get a sense of the directionality of the events, I examine virtual source gathers along approximate lines of receivers in the north-south, east-west, and northeast-southwest directions. I then perform linear moveout on these source gathers using velocities estimated from the tau-p transform to better identify the different events. Finally, I show preliminary results from passive fathometry processing, which appears to retrieve the water-column multiple along with possible reflection events.

FORTIES CONTINUOUS RECORDINGS

The Forties data set, provided to SEP by the Apache Corporation, consists of three groups of ocean-bottom nodes (OBNs) centered at three different platforms in the North Sea. The four-component nodes were deployed as part of an active seismic survey aimed at imaging shallow gas pockets that could pose potential drilling hazards. The nodes were continuously recording, and because active seismic shooting had to be suspended for a couple of days due to severe weather conditions, there were enough quiet periods for ambient noise studies. Furthermore, Brooks and Gerstoft (2009) showed that stormy weather produces more breaking waves at the sea surface, which enable better extraction of vertically-propagating energy in the water column.

For this study, I examine the hydrophone and vertical-geophone components of the Bravo group of OBNs. This cluster of OBNs consists of 52 nodes arranged in a hexagonal shape and centered around an operating platform (Figure 1). The average node spacing is 50 m, and the maximum array offset is approximately 400 m. Each node continuously records for approximately 4 days at 2 ms sampling and is located roughly 120 m below the sea surface. To prepare the recordings for ambient noise processing, I truncate start times up to the nearest quarter of an hour and truncate the end times down to the nearest quarter of an hour. These times are not the same for all nodes, as they were not all deployed simultaneously. Additionally, I remove all

times that contain clear active seismic shooting. For example, Figure 2a shows the full hydrophone power spectrogram for a node near the platform (centered red star in maps in Figure 1), while Figure 2b shows the hydrophone power spectrogram for the same node after the times of active seismic shooting have been removed. I use the data in the latter figure for ambient noise analysis.

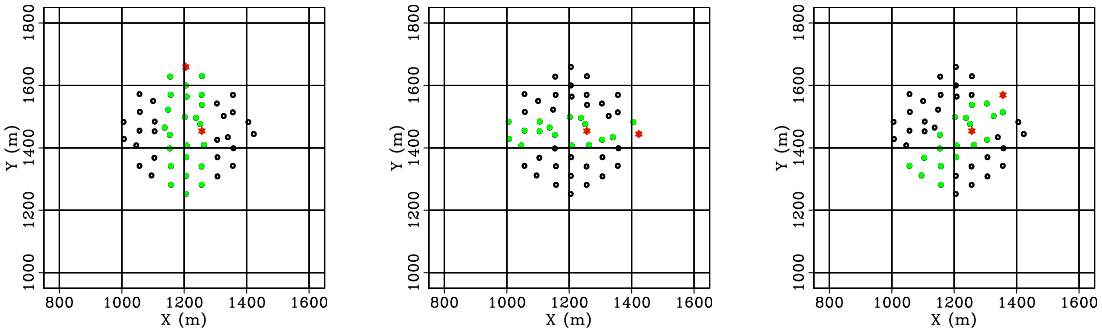

(a) (b) (c)

Figure 1: Maps of nodes at Forties. Red dots indicate virtual source locations. Green dots indicate receivers used for virtual source gathers. The operating platform is located in the center of the array. (a) North-south receiver line. (b) East-west receiver line. (c) Northeast-southwest receiver line. [**CR**]

PASSIVE SEISMIC INTERFEROMETRY

Passive seismic interferometry is performed by cross-correlating the recordings of ambient seismic noise at two receivers. Under certain conditions, the result is an estimate of the Green's function between the two receivers (Wapenaar et al., 2010). By correlating the recording at one receiver with recordings from all other receivers, we can create virtual source gathers.

Processing

I perform the ambient noise cross-correlation technique on the hydrophone and vertical-geophone components of the data. Here, I modify the processing procedure outlined in Chang (2016). To recap, I first ensure that the recordings are synchronized in time and remove all spurious nodes (leaving 49 of 52 nodes). I then divide the recordings into 30-minute time windows with 50% overlap (for a total of 193 time windows, spanning over 2 days). Next, I perform ambient noise cross-correlation by calculating the averaged whitened coherency between each pair of nodes for each time window. This procedure is also referred to as calculating the cross-coherence. In the frequency domain, the procedure is generally expressed as:

$$[G(x_B, x_A, \omega) + G^*(x_B, x_A, \omega)] = \left\langle \left(\frac{U(x_B, \omega)}{\{|U(x_B, \omega)|\}} \right) \left(\frac{U^*(x_A, \omega)}{\{|U(x_A, \omega)|\}} \right) \right\rangle, \qquad (1)$$

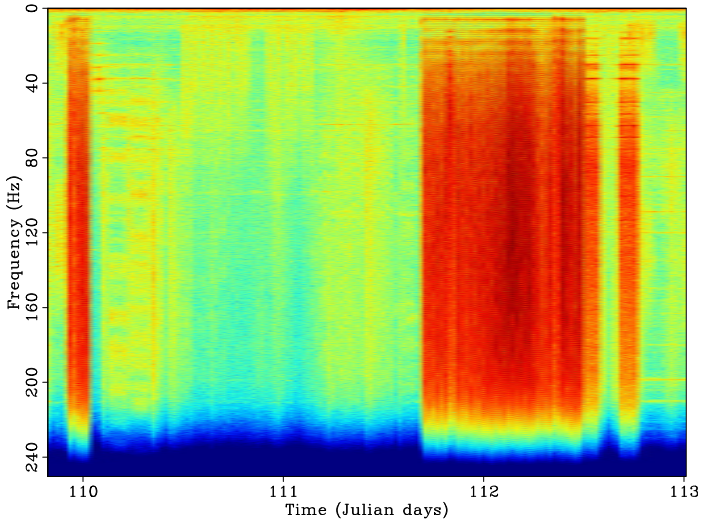

(a)

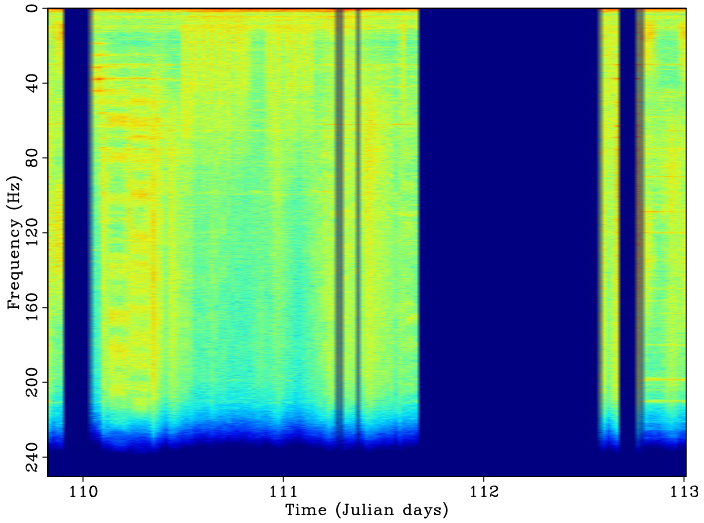

(b)

Figure 2: Power spectrograms for a hydrophone near the platform (centered red star in maps in Figure 1). (a) Full spectrogram. (b) Spectrogram with active sources removed. Power is plotted in log scale. Colors in plots are scaled the same, so they can be compared to each other. [**CR**]

where G is the Green's function between two receiver locations (x_A, x_B), $U(x, \omega)$ is the spectrum of the wavefield at a given receiver location x, $*$ is the complex conjugate, $\langle \cdot \rangle$ is an averaging operation, $| \cdot |$ is the magnitude of the spectrum, and $\{\cdot\}$ is a 0.003 Hz running window average used for normalizing the signal.

The processing procedure here differs from this point on. First, I scale the output of each correlation by the inverse of its maximum amplitude as an extra effort to suppress the effect of potential spurious instrument spikes and sudden large-amplitude events. I then perform phase-weighted stacking across all time windows rather than the traditional linear stack. Phase-weighted stacking is a method that suppresses incoherent noise better than a linear stack, and can thus be effective at detecting weak but coherent arrivals (Schimmel and Paulssen, 1997). The method essentially weighs each time sample from the linear stack by a stack based on the corresponding instantaneous phase (called a phase stack). Specifically, the weight is the stack of the corresponding sample-by-sample-normalized analytic traces. In equation form, the phase-weighted stacking procedure is expressed as:

$$p(t) = \frac{1}{N} \sum_{j=1}^{N} s_j(t) \left| \frac{1}{N} \sum_{k=1}^{N} \exp\left[i \Phi_k(t) \right] \right|^v , \tag{2}$$

where $p(t)$ is the phase-weighted stack result, N is the number of traces being stacked, $s_j(t)$ are the traces being stacked, $\Phi_k(t)$ is the instantaneous phase of the trace, and v is a phase sharpness factor (chosen empirically here to have a value of 2). Thus, time samples with incoherent instantaneous phase are weighted toward 0, while time samples with coherent instantaneous phase are weighted toward 1. Though this stack is not a linear process, the consistent signal in the stack should not be distorted much, while incoherent noise in the stack is damped to allow weaker coherent signals to become more apparent. I use this processing procedure to enhance the apparent P-waves in the virtual source gathers from Chang (2016).

Virtual source gathers

I first create source gathers with a virtual source located near the platform (centered red star in maps in Figure 1) for frequencies between 40 and 80 Hz. Traces are sorted by absolute offset. To compare the effects of different processing on virtual source gathers, I plot the results from processing with linear stacking from Chang (2016) and with phase-weighted stacking (described in the previous section). Compared to the former processing procedure (top row, Figure 3), phase-weighted stacking (bottom row, Figure 3) appears to sharpen the events in the virtual source gathers. The non-linear stacking procedure appears to particularly reduce noise in the vertical-vertical geophone correlations (right column, Figure 3), allowing the secondary event at later positive time lags to become more apparent. Though phase-weighted stacking appears to weaken the dominant arrivals in the hydrophone-hydrophone correlations (left column, Figure 3), it seems to also dampen the overall amount of noise as well

as reveal a faster-propagating event at positive times lags not apparent in the original processing procedure.

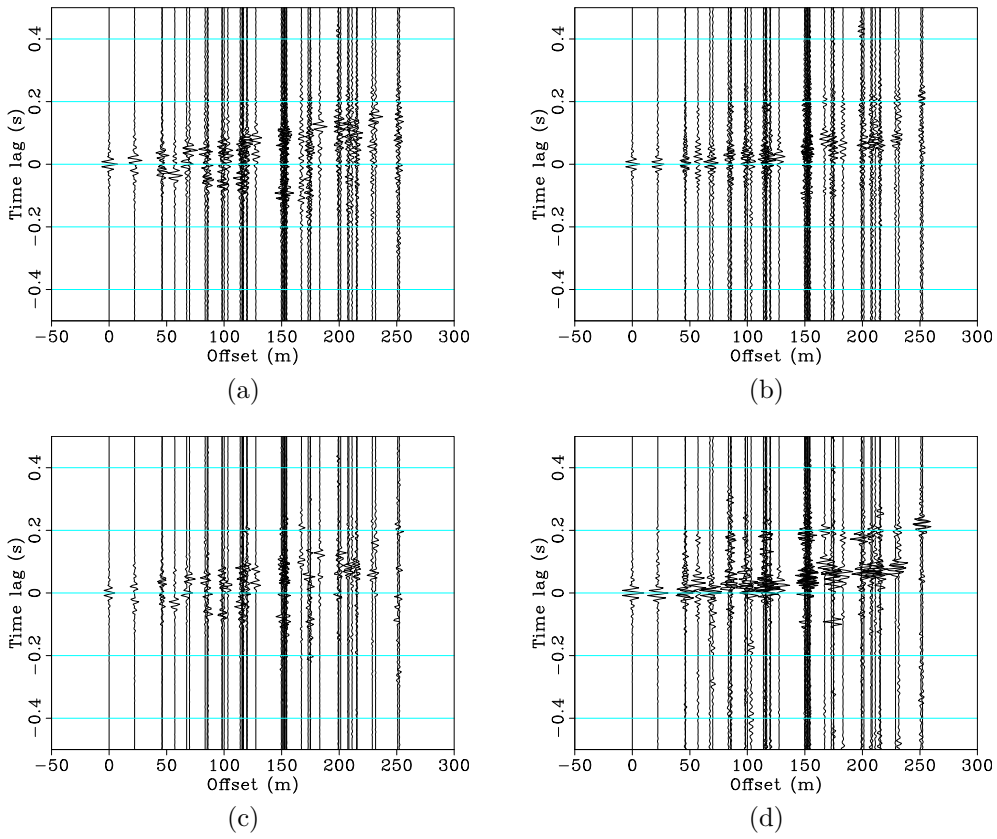

Figure 3: Source gathers for frequencies between 40 and 80 Hz with the virtual source located near the platform (centered red star in maps in Figure 1). Traces are sorted by absolute offset. Top row: cross-coherence processing with linear stacking. Bottom row: cross-coherence processing with temporal normalization and phase-weighted stacking. Left column: hydrophone-hydrophone correlations. Right column: vertical-vertical geophone correlations. [**CR**]

Overall, we see clear arrivals in the correlations from both components. Looking at the hydrophone-hydrophone correlations (left column, Figure 3), we see significant energy at both positive and negative time lags. This suggests that there is seismic energy not only traveling away from the platform (as expected), but there is also a significant amount of energy traveling toward the platform. Additionally, while the phase-weighted stack may appear to degrade the phase at far offsets, it does reveal hints of a faster-propagating event at positive time lags not clearly observed when a linear stack is employed. By performing a tau-p transform on the hydrophone-hydrophone correlations (Figure 4a), I estimate that the primary event is propagating at approximately 1500 m/s (0.00067 s/m), while the faster event is propagating at approximately 3000 m/s (0.00033 s/m). Both events appear to have 0 s intercept time. Looking at the vertical-vertical geophone correlations (right column, Figure 3), there are two clear events at positive time lags. This suggests that both events are generated

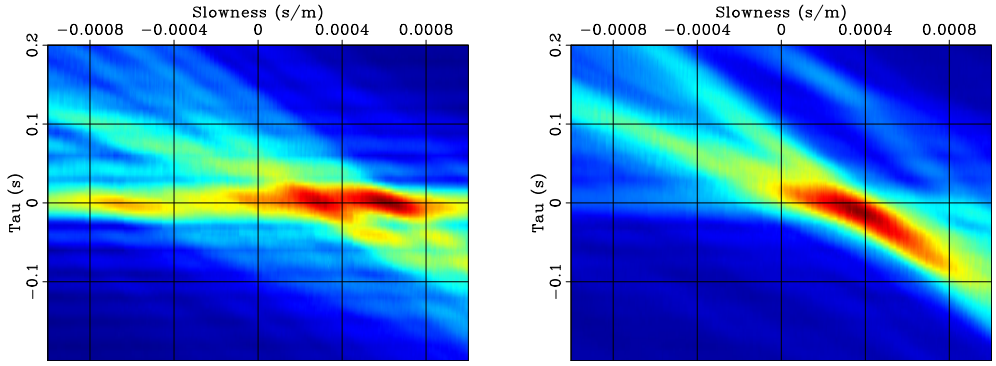

(a) (b)

Figure 4: Tau-p transforms of the phase-weighted stacked virtual source gathers (bottom row, Figure 3). (a) Hydrophone-hydrophone correlations. (b) Vertical-vertical geophone correlations. Warmer colors indicate higher stacking power in the tau-p domain. The weaker event around intercept time 0.14 s and slowness 0.00033 s/m in (b) is likely related to the secondary event in Figure 3d. [**CR**]

by the platform. By performing a tau-p transform on the vertical-vertical geophone correlations (Figure 4b), I estimate that both events are propagating at approximately 3000 m/s (0.00033 s/m), which is similar to the velocity of the faster event in the hydrophone-hydrophone correlations that was enhanced by phase-weighted stacking. Note that the secondary event around intercept time 0.14 s and slowness 0.00033 s/m in the tau-p transform is very weak compared to the primary event. I also estimate that the intercept time of the primary event is 0 s, while the intercept time of the weaker secondary event is approximately 0.15 s. Thus, from these virtual source gathers and the corresponding analysis, I determine that there are three different types of events:

1. A linear event propagating at 1500 m/s towards and away from the platform, observed in the hydrophone-hydrophone correlations (Figure 3c).

2. A linear event propagating at 3000 m/s with 0 s intercept time away from the platform, observed in both the hydrophone-hydrophone and vertical-vertical geophone correlations (Figures 3c and 3d, respectively).

3. A weaker linear event propagating at 3000 m/s with 0.15 s intercept time away from the platform, observed in the vertical-vertical geophone correlations (Figure 3d; most evident at far offsets).

To get a better sense of the directionality (not just towards and away from the platform), I create virtual source gathers with approximate lines of receivers in the north-south, east-west, and northeast-southwest directions (maps in Figure 1). All source gathers here use phase-weighted stacking rather than linear stacking. I first examine source gathers along the north-south direction with a virtual source located

in the north of the array. From the hydrophone-hydrophone correlation (Figure 5a), we can see two types of events. At positive time lags, we see a clear event moving away from the virtual source. This suggests that this particular event is not moving north from the platform, but is moving south toward the platform. Because energy is moving away from the virtual source, I perform linear moveout (LMO) centered at the virtual source location using the previously estimated velocity of 1500 m/s from the tau-p transform and find that it flattens this particular event (Figure 5b). At negative time lags we see a faster event with a V shape indicative of a strong source in the array (Chang et al., 2016). The peak of the V shape is located near the center of the array, which is where the platform is approximately located. Because energy appears to move away from the platform location, I perform LMO centered at the platform location (about -200 m offset) with a velocity of 3000 m/s to flatten this particular event (Figure 5c). Looking at the vertical-vertical geophone correlations (Figure 5d), we see that nearly all the energy is at negative time lags and that the moveout of both events follow a V shape centered at the platform location. Again, performing LMO with a velocity of 3000 m/s centered at the platform location flattens these particular events (Figure 5e).

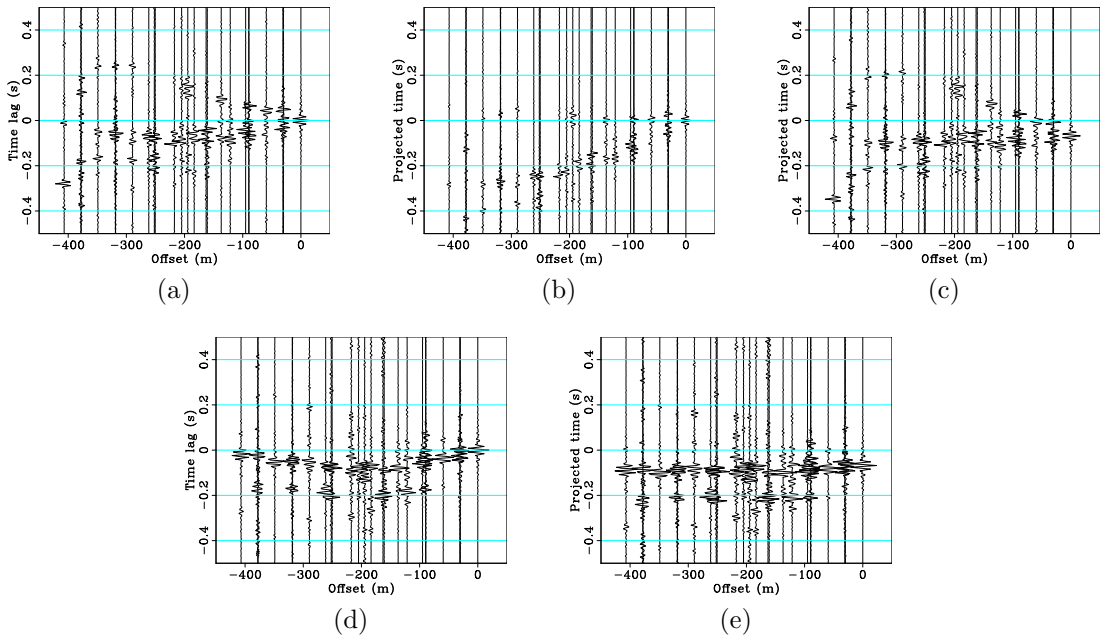

Figure 5: Virtual source gathers after phase-weighted stacking for frequencies between 40 and 80 Hz with receivers along approximate lines in the north-south direction. Virtual source is north in the array (see Figure 1a). Top row: hydrophone-hydrophone correlations. (a) Original source gather. (b) Source gather after LMO at 1500 m/s centered at the source location (0 m offset). (c) Source gather after LMO at 3000 m/s centered at the platform location (-200 m offset). Bottom row: vertical-vertical geophone correlations. (d) Original source gather. (e) Source gather after LMO at 3000 m/s centered at the platform location (-200 m offset). Gathers are sorted by offset in the north-south direction. [**CR**]

Similar observations can be made when looking at source gathers with an apparent line of receivers in the east-west direction and a virtual source in the east of the array. In the hydrophone-hydrophone correlations (Figure 6a), we can again see two events: the linear event moving away from the virtual source (toward the west), and the V-shaped event at negative time lags centered at the platform location. Performing LMO with a velocity of 1500 m/s centered at the source location flattens the event at positive time lags (Figure 6b). Performing LMO with a velocity of 3000 m/s centered at the platform location (about -200 m offset) flattens the event at positive time lags (Figure 6c). Much like the north-south correlations, we can see two events at negative time lags in the vertical-vertical correlations along the east-west direction (Figure 6d). Again, performing LMO with a velocity of 3000 m/s centered at the platform location flattens these two events (Figure 6e).

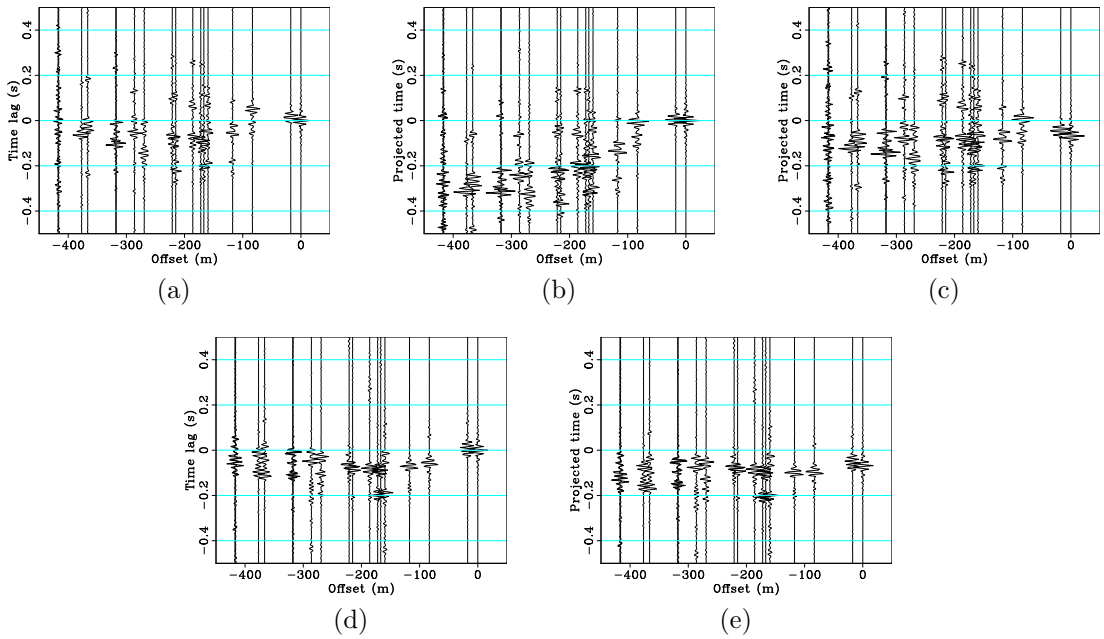

Figure 6: Virtual source gathers after phase-weighted stacking for frequencies between 40 and 80 Hz with receivers along approximate lines in the east-west direction. Virtual source is east in the array (see Figure 1b). Top row: hydrophone-hydrophone correlations. (a) Original source gather. (b) Source gather after LMO at 1500 m/s centered at the source location (0 m offset). (c) Source gather after LMO at 3000 m/s centered at the platform location (-200 m offset). Bottom row: vertical-vertical geophone correlations. (d) Original source gather. (e) Source gather after LMO at 3000 m/s centered at the platform location (-200 m offset). Gathers are sorted by offset in the east-west direction. [**CR**]

Given that the slower event in the hydrophone-hydrophone correlations appears to propagate at water velocity along the south and west directions, I examine source gathers with a virtual source in the northeast of the array and an apparent line of receivers along the northeast-southwest direction. The goal is to determine if the energy is propagating toward the southwest from a distinct source in the northeast

or propagating along a number of azimuths between due south and due west. As in the hydrophone-hydrophone correlations along the other two directions, we see that there are two clear events: the linear event moving away from the virtual source (toward the southwest), and the faster event at negative time lags. Performing LMO with a velocity of 1500 m/s centered at the source location again flattens the event at positive time lags (Figure 7b). Therefore, it appears that this particular event propagates at water velocity (not slower than water velocity) along the northeast-southwest direction. This suggests that this event does not originate from a single source in the northeast, but rather originates from a number of sources along azimuths between due north and due east (leading to propagation along azimuths between due south and due west, respectively). For completeness, I also perform LMO centered at the virtual source with a velocity of 3000 m/s to flatten the faster event at negative time lags (Figure 7c). As for the vertical-vertical geophone correlations, the results are similar to those from the other two apparent lines of receivers. There are multiple events that appear to originate from the platform location (Figure 7d), and performing LMO centered at the platform with a velocity of 3000 m/s appears to flatten those events (Figure 7e).

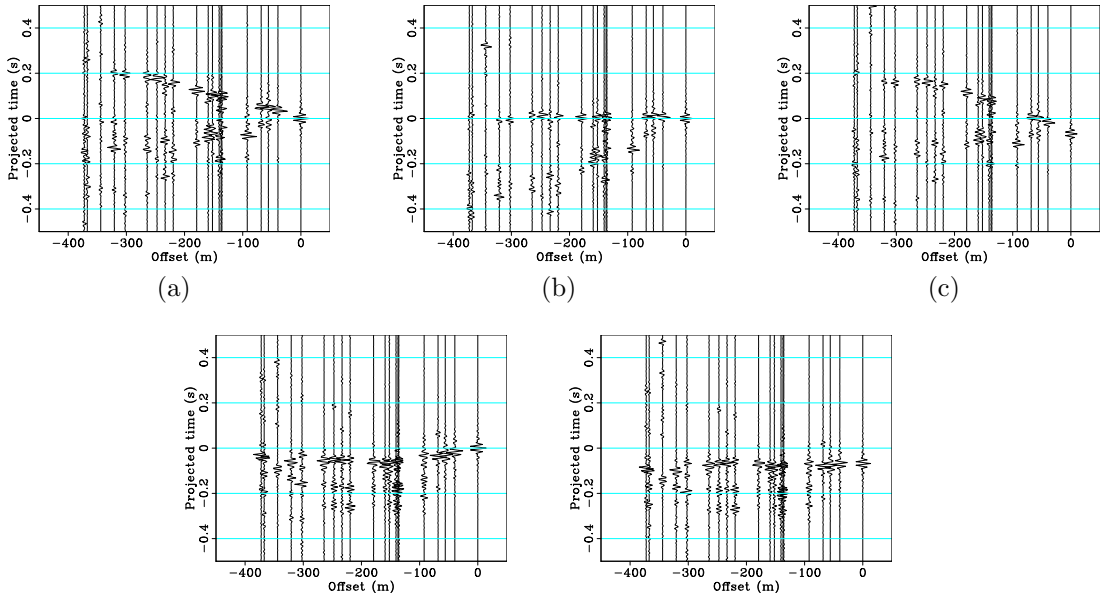

Figure 7: Virtual source gathers after phase-weighted stacking for frequencies between 40 and 80 Hz with receivers along approximate lines in the northeast-southwest direction. Virtual source is northeast in the array (see Figure 1b). Top row: hydrophone-hydrophone correlations. (a) Original source gather. (b) Source gather after LMO at 1500 m/s centered at the source location (0 m offset). (c) Source gather after LMO at 3000 m/s centered at the platform location (-200 m offset). Bottom row: vertical-vertical geophone correlations. (d) Original source gather. (e) Source gather after LMO at 3000 m/s centered at the platform location (-200 m offset). Gathers are sorted by offset in the northeast-southwest direction. [**CR**]

Therefore, from these virtual source gathers, we can elaborate on each of the three previously mentioned events:

1. The linear event propagating at 1500 m/s observed in the hydrophone-hydrophone correlation appears to be arriving from outside the array and propagating along multiple azimuths between due south and due west.
2. The linear event propagating at 3000 m/s with 0 s intercept time observed in both the hydrophone-hydrophone and vertical-vertical geophone correlations is generated by the platform.
3. The linear event propagating at 3000 m/s with 0.15 s intercept time observed in the vertical-vertical geophone correlations is also generated by the platform.

Given the apparent velocities and directions of these three events, we are likely looking at acoustic P-waves traveling in the water or body waves. The event traveling at 1500 m/s is potentially energy moving horizontally across the array at water velocity, which would explain why this event is so weak in the vertical-vertical geophone correlations. The origin of this signal could be some distant sources between due north and due east of the array. Since the sea-surface and sea-bottom act as a waveguide, signals from distant sources experience little attenuation and typically display mostly horizontally-propagating wavefronts (Brooks and Gerstoft, 2009). One potential source is distant shipping noise, which dominates the marine ambient seismic noise field at frequencies between 25 and 250 Hz (Wenz, 1972). Another potential source is active seismic shooting from another survey in the North Sea.

As for the events traveling at 3000 m/s, it is likely to be energy traveling with some vertical component of movement, as it is observed in both the hydrophone-hydrophone and vertical-vertical geophone correlations. Though it could be energy propagating through the subsurface, it seems more likely that it is energy traveling through the water. This is because the secondary event propagating at 3000 m/s in the vertical-vertical geophone correlations has an intercept time of approximately 0.15 s, which is approximately the two-way traveltime of a vertically-propagating event traveling through a water column 120 m deep at 1500 m/s. Additionally, the source of this high-velocity event appears to be the platform. Given that there was a severe storm during the continuous recordings, it is possible that ocean waves crashing against the platform could produce these types of events. Given an apparent velocity of 3000 m/s and assuming a plane wave traveling through the water at 1500 m/s, P-wave energy would be hitting the array at approximately 30 degrees with respect to normal. Assuming there is some vertical component to these high-velocity events, there is potential to obtain subsurface reflections. I turn to passive fathometry processing in an attempt to extract these types of reflections from the ambient seismic noise field.

PASSIVE FATHOMETRY

Passive fathometry is based on the idea that the cross-correlation of energy generated from breaking waves at the sea surface and its echo return from the seabed can be used to estimate travel times to subsurface reflectors (Gerstoft et al., 2008; Siderius et al., 2010). Therefore, the technique is similar to passive seismic interferometry in that they are both based on the cross-correlation of noise wavefields. Here, I apply passive fathometry processing on individual receivers in an attempt to extract reflection profiles beneath select OBNs.

Processing

Passive fathometry has been successfully applied to vertical arrays of hydrophones and geophones in shallow marine environments (Gerstoft et al., 2008; Siderius et al., 2010). The orientation of these arrays allowed for efficient separation of up- and down-going events using an adaptive beamforming approach. The cross-correlation of these two events can produce a reflection sequence beneath the array. Here, I adapt this processing procedure for use with horizontally-oriented ocean-bottom arrays.

Many ocean-bottom arrays contain both vertical-geophone and hydrophone components, making it possible to perform up- and down-going wavefield separation using PZ summation. In the acoustic decomposition (Schalkwijk et al., 1999), the up- and down-going pressure wavefields are obtained by:

$$P_{\text{up}}(\omega,k) = \frac{1}{2}\left[P(\omega,k) + a(\omega)\frac{\rho}{q(\omega,k)}Z(\omega,k)\right] \ , \tag{3}$$

and

$$P_{\text{down}}(\omega,k) = \frac{1}{2}\left[P(\omega,k) - a(\omega)\frac{\rho}{q(\omega,k)}Z(\omega,k)\right] \ , \tag{4}$$

respectively, where P is the pressure component, Z is the vertical velocity component, ω is frequency, k is horizontal wavenumber, ρ is density of water, and q is vertical slowness in the water layer defined as $q(\omega,k) = \sqrt{c^{-2} - p^2(\omega,k)}$, where c is water velocity and p is the ray parameter.

I am interested in passive up-down separation at each individual node (not between nodes). For this report, I will assume that passive energy arrives at near-vertical incidence. This assumption allows some simplifications when estimating the calibration filter for PZ summation using active-source seismic data. First, I can focus on performing up-down separation on the zero-offset trace rather than the entire gather. Second, I can take the vertical slowness in the water layer to be the inverse of water velocity. Equations 3 and 4 thus simplify to:

$$P_{\text{up}}(\omega) = \frac{1}{2}\left[P(\omega) + a(\omega)\rho c Z(\omega)\right] \ , \tag{5}$$

and

$$P_{\text{down}}(\omega) = \frac{1}{2}\left[P(\omega) - a(\omega)\rho c Z(\omega)\right] \ . \tag{6}$$

To estimate the calibration filter, I follow the approach from Biondi and Levin (2014) to estimate the calibration filter from the zero-offset active-source data. This filter is typically estimated by minimizing the energy of the down-going pressure field in a window containing only up-going events. Here, I use a time window around a reflection event in the active-source data rather than a refraction event. First, I remove the instrument response from both the hydrophone and vertical-geophone recordings. Second, I manually select a time window around a reflection event near zero-offset for each node of interest. Finally, I compute a Wiener shaping filter that shapes the vertical-component reflection to the reflection recorded by the hydrophone within the picked window. This particular filter incorporates the density and slowness factors in Equations 5 and 6.

An example of the result of acoustic up-down separation on active source data is shown in the common receiver gathers for the receiver in the north of the array in Figure 8. Gathers have been bandpassed for frequencies between 20 and 220 Hz. Though the calibration filter is only applied to a time window in the zero-offset trace, the acoustic decomposition appears to be fairly effective throughout the gathers. The reflections just after the direct arrival are apparent in the upgoing pressure wavefield and nearly non-existent in the downgoing pressure wavefield. Additionally, the first water-column multiple (approximately 0.26 s at zero-offset) is weaker in the upgoing pressure wavefield than in the downgoing pressure wavefield.

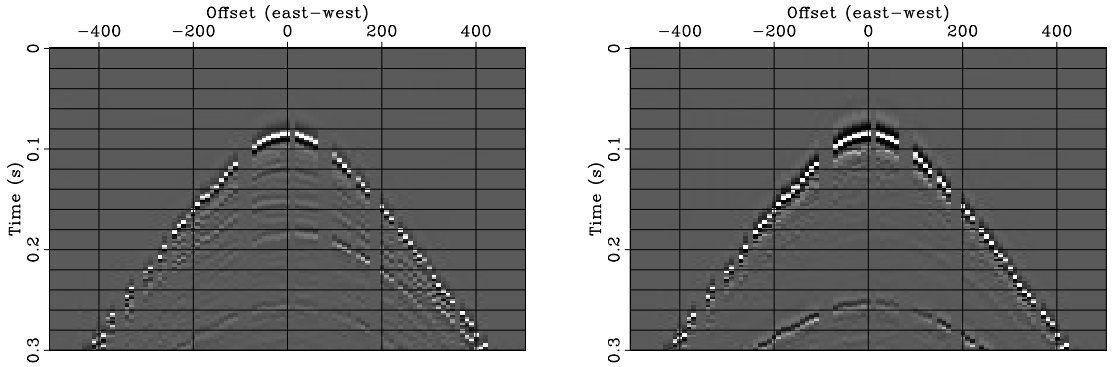

(a) (b)

Figure 8: Common receiver gathers from active-source data for a receiver in the north of the array after acoustic up-down separation. (a) Upgoing acoustic wavefield. (b) Downgoing acoustic wavefield. Gathers are bandpassed for frequencies between 20 and 220 Hz. [**CR**]

With a reasonable calibration coefficient between the hydrophone and vertical-geophone recordings, I apply the same up-down separation processing to the same 30-minute time windows used for seismic interferometry in the previous section. As with the active source data, I first remove the instrument responses from the passive

recordings. I then bandpass the recordings for frequencies between 20 and 220 Hz. Typical passive fathometry uses acoustic energy up to kHz, so I examine up to fairly high frequency here. I then perform PZ summation on the passive recordings using the corresponding calibration coefficient for each node. Finally, I correlate the resulting up- and down-going wavefields from each time window and combine them with a phase-weighted stack.

1D profiles

Preliminary results from passive fathometry are shown for four node locations in Figure 9. A gain function t has been applied to each of the 1D profiles to limit the spike at zero-lag time and to enhance later arrivals. All of the 1D profiles share similar traits. One of the prominent events is the apparent arrival between 0.14 and 0.16 s. As discussed previously, the water depth in this area is approximately 120 m. Assuming a water velocity of 1500 m/s, the water-column multiple would take about 0.16 s to travel up and down. Additionally, there appears to consistently be an event between 0.3 and 0.32 s, which could be related to the second water-column multiple (two trips up and down). It should be noted that while these events arrive at the expected times of the water-column multiples, they do not display the expected opposite polarity. More investigation is needed to address this characteristic, as it might help determine whether these events are indeed water-column multiples. While there appear to be a few arrivals between the potential water-column multiples in each of the profiles, their arrival times do not obviously correspond to any events in the active-source data.

Furthermore, there appears to be an event before the first apparent water-column multiple, which is when we would expect to observe any near-surface reflections. Whether this event at 0.08 s is an actual reflection remains to be determined. The arrival time is consistent in all fathometry results, which could indicate a flat reflector or be an artifact of processing. Additionally, this is the only clear event before the first water-column multiple, whereas the active-source data reveals multiple reflections before the first multiple. A careful comparison with the active-source data will be required to determine whether these preliminary fathometry results are indeed identifying subsurface reflection events. Overall, passive fathometry processing appears to extract the water-column multiples as well as potential reflection events.

Clearly, there can be improvements to the method. One improvement would be the development of a spatial filter that could use the geometry of arrays to isolate vertically-propagating energy. The current method assumes that most of the energy is vertically-propagating. This would be true if most of the energy at these frequencies were actually generated by breaking waves at the sea surface. However, this is unlikely to be a valid assumption (particularly for stations further from the platform) given that the platform appears to be a dominant source of energy, and given that shipping noise is the dominant source of energy at these frequencies. Another improvement would be to use only times when there was a storm. As shown in Brooks and Gerstoft (2009), more vertically-propagating events are extracted during periods when waves

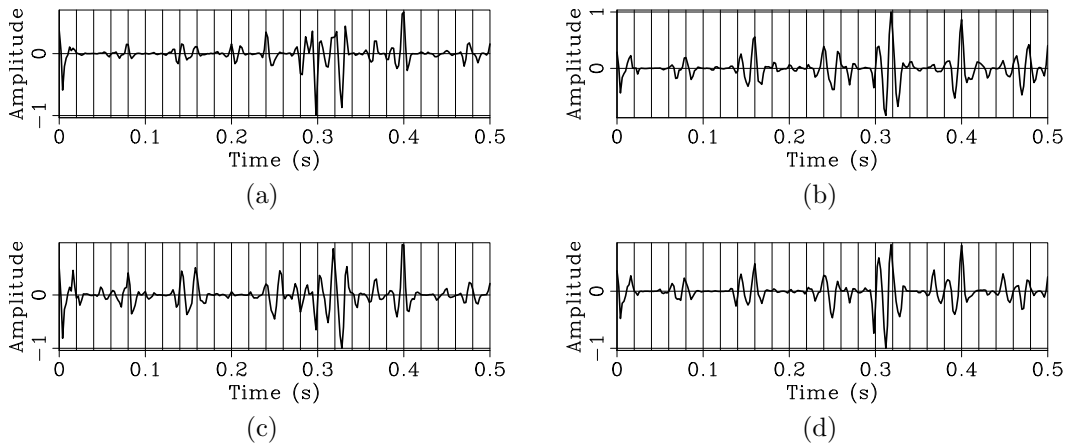

Figure 9: Results from passive fathometry at four different node locations. (a) Southwest edge in the array. (b) North edge in the array (corresponding to the receiver location in Figure 8). (c) East edge in the array. (d) Southwest near the platform. Results are for frequencies between 20 and 220 Hz. Gain function t is applied to limit the spike at zero-lag time and to enhance later arrivals. [**CR**]

are breaking violently. Though this would result in the use of less recording time, I would only be using times when the desired signal would theoretically be strong. Overall, passive fathometry appears to be picking up possible physical events, which is a promising development for any future investigation into P-waves at Forties.

CONCLUSIONS

I investigated the apparent P-waves in the ambient seismic noise recordings from Apache Forties using seismic interferometry and passive fathometry processing. By using a phase-weighted stack in the seismic interferometry workflow, I showed that there are three apparent events in the hydrophone-hydrophone and vertical-vertical geophone correlations. I used tau-p transforms and virtual source gathers with approximate lines of receivers to determine the velocity and directionality of these events. One event travels at 1500 m/s and appeared to travel across the array along azimuths between due south and due west. Because it is most apparent in the hydrophone-hydrophone correlations, I hypothesized that this event was a horizontally-propagating event likely originating from distant sources between due north and due east. Another event traveled at approximately 3000 m/s with 0 s intercept time, and appeared in the correlations from both components. The last event also traveled at approximately 3000 m/s but with 0.15 s intercept time, and appeared in only the vertical-vertical geophone correlations. I hypothesized that the origin of these events was the platform, and that they were likely reverberations in the water column. Given this interpretation of the faster events, I performed passive fathometry processing on the ambient noise in an attempt to harness vertically-propagating energy for extracting subsurface reflections. Preliminary results suggest that I again

recovered the water-column multiple, as well as possible subsurface reflections.

ACKNOWLEDGMENTS

The author would like to thank Apache North Sea Limited for access to the data set and permission to publish. The author also thanks Biondo Biondi, Shuki Ronen, Bob Clapp, and Stewart Levin for help processing the data and useful discussions. Finally, the author would like to thank the sponsors of the Stanford Exploration Project for their financial support.

REFERENCES

Bensen, G., M. Ritzwoller, and N. Shapiro, 2008, Broadband ambient noise surface wave tomography across the United States: Journal of Geophysical Research: Solid Earth, **113**.

Biondi, E. and S. A. Levin, 2014, Up-down separation of ocean bottom node data using calibration filter based on critically refracted waves and adaptive subtraction: SEP-Report, **155**.

Brooks, L. A. and P. Gerstoft, 2009, Green's function approximation from cross-correlations of 20–100 Hz noise during a tropical storm: The Journal of the Acoustical Society of America, **125**, 723–734.

Chang, J., 2016, Multicomponent ambient noise crosscorrelation at Forties: 86th Annual International Meeting, SEG, Expanded Abstracts, 2709–2714.

Chang, J. P., S. A. de Ridder, and B. L. Biondi, 2016, High-frequency Rayleigh-wave tomography using traffic noise from Long Beach, California: Geophysics, **81**, B1–B11.

de Ridder, S. and J. Dellinger, 2011, Ambient seismic noise eikonal tomography for near-surface imaging at Valhall: The Leading Edge, **30**, 506–512.

Draganov, D., X. Campman, J. Thorbecke, A. Verdel, and K. Wapenaar, 2013, Seismic exploration-scale velocities and structure from ambient seismic noise (¿ 1 Hz): Journal of Geophysical Research: Solid Earth, **118**, 4345–4360.

Gerstoft, P., W. S. Hodgkiss, M. Siderius, C.-F. Huang, and C. H. Harrison, 2008, Passive fathometer processing: The Journal of the Acoustical Society of America, **123**, 1297.

Mordret, A., M. Landès, N. Shapiro, S. Singh, P. Roux, and O. Barkved, 2013, Near-surface study at the valhall oil field from ambient noise surface wave tomography: Geophysical Journal International, ggt061.

Nakata, N., J. P. Chang, J. F. Lawrence, and P. Boué, 2015, Body wave extraction and tomography at long beach, california, with ambient-noise interferometry: Journal of Geophysical Research: Solid Earth, **120**, 1159–1173.

Nakata, N., R. Snieder, T. Tsuji, K. Larner, and T. Matsuoka, 2011, Shear wave imaging from traffic noise using seismic interferometry by cross-coherence: Geophysics, **76**, SA97–SA106.

Schalkwijk, K., C. Wapenaar, and D. Verschuur, 1999, Application of two-step decomposition to multicomponent ocean-bottom data: Theory and case study: Journal of Seismic Exploration, **8**, 261–278.

Schimmel, M. and H. Paulssen, 1997, Noise reduction and detection of weak, coherent signals through phase-weighted stacks: Geophysical Journal International, **130**, 497–505.

Shapiro, N. M., M. Campillo, L. Stehly, and M. H. Ritzwoller, 2005, High-resolution surface-wave tomography from ambient seismic noise: Science, **307**, 1615–1618.

Siderius, M., H. Song, P. Gerstoft, W. S. Hodgkiss, P. Hursky, and C. Harrison, 2010, Adaptive passive fathometer processing: The Journal of the Acoustical Society of America, **127**, 2193.

Wapenaar, K., D. Draganov, R. Snieder, X. Campman, and A. Verdel, 2010, Tutorial on seismic interferometry: Part 1–basic principles and applications: Geophysics, **75**, 75A195–75A209.

Wenz, G. M., 1972, Review of underwater acoustics research: Noise: The Journal of the Acoustical Society of America, **51**, 1010–1024.